JOURNAL OF GEOPHYSICAL RESEARCH, VOL. 102, NO. B2, PAGES 2969–2981, FEBRUARY 10, 1997

Monte Carlo analysis of seismic reflections from Moho and the W reflector

Klaus Mosegaard

Dept. of Geophysics, Niels Bohr Institute for Astronomy, Physics and Geophysics, Copenhagen Denmark

Satish Singh and David Snyder

British Institutions Reflection Profiling Syndicate, Bullard Laboratories, University of Cambridge Cambridge, England

Helle Wagner

Dept. of Geophysics, Niels Bohr Institute for Astronomy, Physics and Geophysics, Copenhagen Denmark

Abstract. Near-normal-incidence reflections have been used to image the Moho and the W reflector structure in the lithosphere, offshore northern Scotland. To determine the impedance variations at these reflectors, we use a Monte Carlo technique which allows incorporation of geologically realistic a priori information as well as an extensive exploration of the model space, after testing it on a synthetic data set. The method is based on Bayesian inversion theory. The modeled Moho consists of a series of layers with a total thickness of $\sim 2.4 \pm 0.3$ km with an overall positive impedance contrast. Inversion of the W reflector results in a model of five-seven layers with a total thickness of about 3.7 ± 0.6 km and mostly nonpositive impedance contrasts. The implied fine-scale impedance structure of the Moho is consistent with the broader velocity structure determined from previous wide-angle reflection/refraction profiles. However, the overall nonpositive impedance contrast at the W reflector requires a structure which is overlain or underlain by a broad increase in velocity in order to match amplitudes of reflected phases observed at large offsets interpreted previously to originate at a similar depth.

Introduction

In the last few decades, deep seismic reflection profiling has provided spectacular images of the continental lithosphere worldwide, of which subhorizontal reflections from the lower crust, reflections from the Moho, and reflections from the upper mantle have been particularly notable. Some reflections have been associated with known structures; for example, bright reflections near the Moho depth have been associated with the crust-mantle transition zone, and dipping reflections in the crust have been associated with near surface faults and known subduction zones [*Klemperer and Hobbs,* 1991; *Clowes et al.,* 1992; *BABEL Working Group,* 1993; *Zhao et al.,* 1993; *Clowes and Green,* 1994]. Many features, mainly subhorizontal ones, remain incompletely understood. Although various models have been proposed for these features, one ultimately requires outcrops, drill holes, or the physical properties (density and seismic velocity) of these reflectors to choose from among these models. Deep seismic reflections, as such, are incapable of providing direct information on physical properties. Instead, one derives some estimates of the physical properties from the seismic record using a modeling strategy.

Conventional seismic data processing allows a comparatively fast but rough analysis of large volumes of seismic data. It is essentially based on a linear model of the seismic trace, the so-called convolutional model, in which the seismic trace $s(t)$ is approximated by a convolution of the subsurface reflectivity $r(t)$ and a source wavelet $w(t)$:

$$s(t) = w(t) * r(t)$$

According to the convolution theorem, one consequence of this approximate model is that only those frequencies that are present in the source wavelet can be retrieved from the reflectivity series of a recorded seismic trace. Seismic sources used in conventional deep seismic marine experiments typically have 5 to 80-Hz bandwidths [*Hobbs and Snyder,* 1993]. Due to attenuation, a seismic wavelet at a given two-way time will have little energy above 60 Hz, and the convolutional model alone cannot

Paper number 96JB02566.
0148-0227/97/96JB-02566$09.00

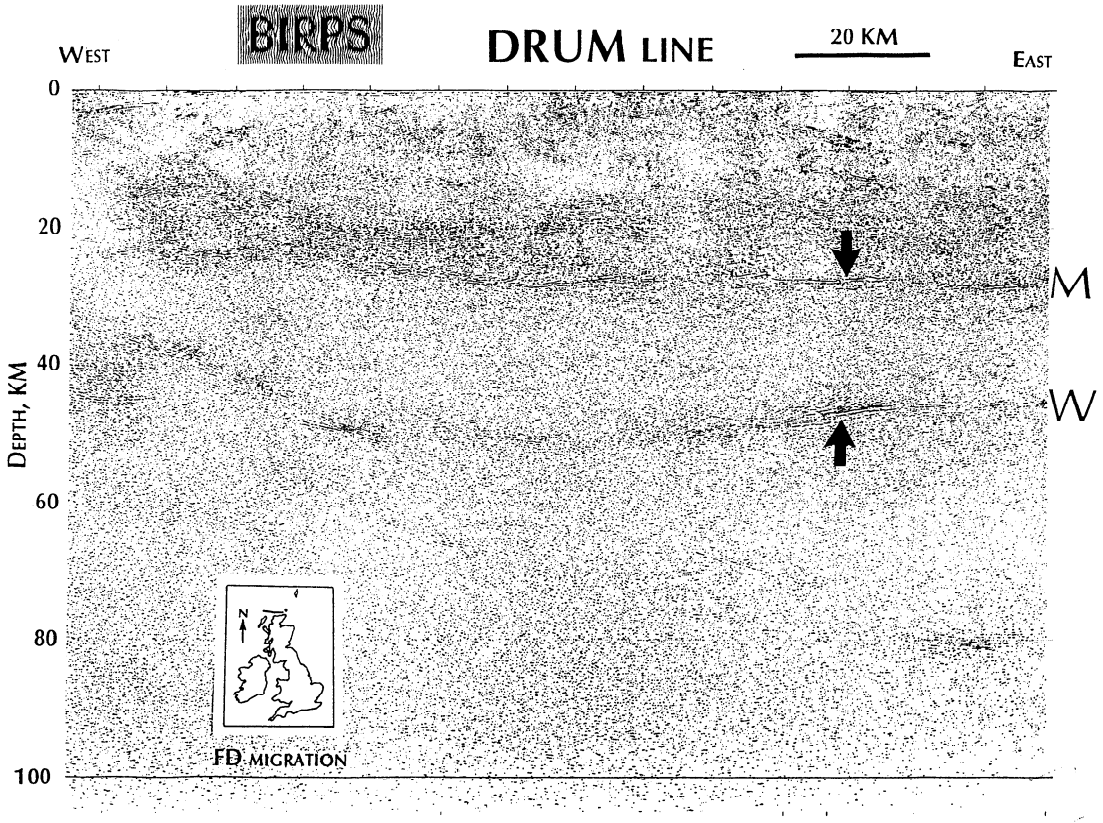

Figure 1. The DRUM seismic section showing the Moho (M) and W (W) reflectors and the location of the data used in the Monte Carlo inversion. The section was migrated using a two-dimensional velocity field derived from nearby refraction results [*Snyder and Flack,* 1990] and then depth converted using the same velocities. The Flannan reflector can also be observed, dipping from 30-km depths at the western edge of the profile to 80-km depths in the east.

provide any information about the reflectivity at spatial frequencies equivalent to ≥ 60 Hz at that two-way time. At frequencies less than 5 Hz, reflected seismic energy is normally absent or obscured by ship noise. Consequently, the convolutional model is unable to predict any low-degree trend or nonzero average value of the reflectivity.

If one is interested in extracting information outside the limited passband of the source wavelet, it is necessary to incorporate a priori information about the subsurface, abandon the convolutional model and replace it with the correct relationship between seismic data and Earth model. In this paper, we propose a framework under which variations in impedance inside and outside the frequency passband of the seismic wavelet can be estimated by nonlinear inversion using prior information on the model in terms of probabilities. A Monte Carlo inversion technique [*Mosegaard and Tarantola,* 1995] provides models which fit the observed data and estimates errors and resolution of these models. We apply this framework to shot records from the DRUM (Deep Reflections from the Upper Mantle) reflection profile from the north of Scotland to estimate impedance variations at the Moho and at the W reflector (Figures 1 and 2) and to provide estimates of the resolution of these impedances. The DRUM line was designed to investigate the reflectivity of the lower continental lithosphere and was recorded for 30 s two-way travel time (TWT), corresponding to about 110-km depth [*McGeary and Warner,* 1985]. Various dipping reflections are observed in the upper crust (0 to 5 s) and a series of subhorizontal reflections in the lower crust (6 to 9 s), the base of which, at ~ 9 s TWT, coincides with the Moho defined by nearby refraction observations [*Barton,* 1992]. Three strong reflectors occur in the mantle: a subhorizontal reflector around 13-15 s TWT (the W reflector), an easterly dipping reflector (the Flannan reflector) recorded from 9 s down to at least 27 s and possibly 30 s, and a 15-km-long banded zone at 23 s (Figure 1) [*McGeary and Warner,* 1985]. Derivation of the physical properties of these deep reflectors from the seismic records is critical to understanding the formation and evolution of the continental lithosphere around the British Isles.

A Probabilistic Formulation of the Problem

Analysis of the resolution of subsurface structures from seismic data requires a probabilistic formulation of the inverse problem. Due to the often strongly non-

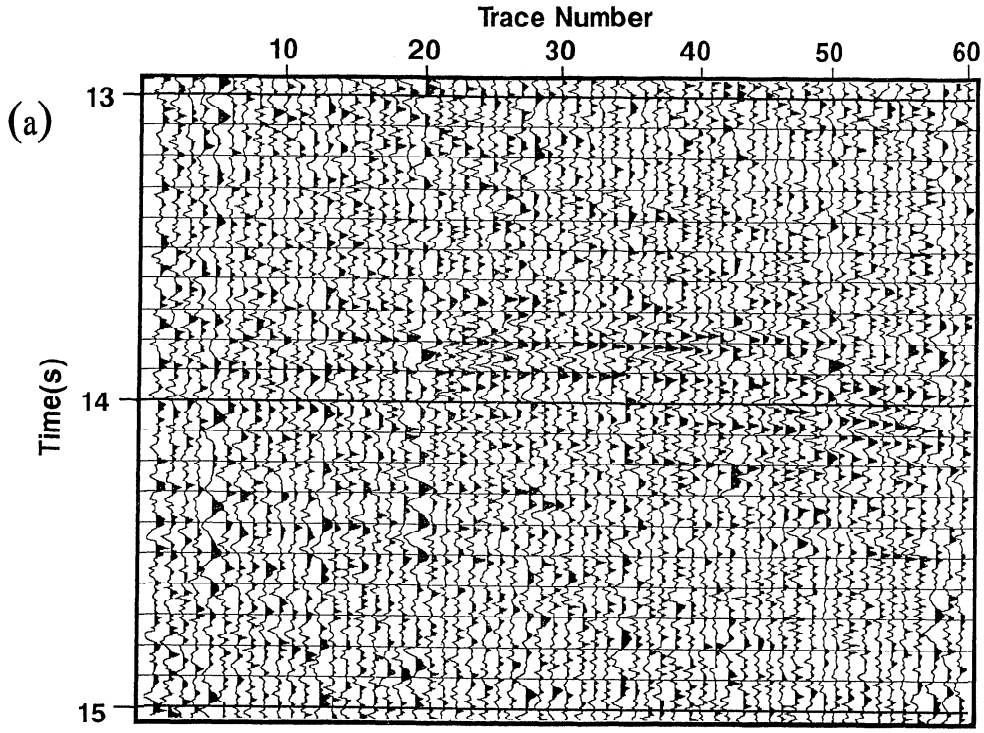

Figure 2. The data used for inversion. (a) The shot gather from 13 to 15 s at shot point 3564 of the DRUM profile, a TWT zone for the W reflector. These 60 traces have increasing offset from left (209 m) to right (3210 m). These traces were summed in groups of six to produce 10 traces with enhanced signal-to-noise ratios for the inversion. (b) The summed traces over the time range of 8-10 s that contains the Moho reflection at about 8.9 s. (c) The summed traces over the the time range of 13-15 s that contains the W reflection at about 13.8 s. (d) Amplitude spectrum of data with Moho reflection. (e) Amplitude spectrum of data with W reflection. (f) Estimated marginal noise distribution for a single data sample (Moho data). The solid curve is a Gaussian distribution. (g) Estimated noise autocorrelation (Moho data).

linear relationship between the subsurface impedance model and seismic data, the distribution of errors in the observed data is mapped into the model space as a complex error distribution. Among the important pathologies of this relationship is an inherent nonuniqueness of models that fit the data. Further complexity is added to the model distribution when we, on geological grounds, must introduce complex, data-independent a priori information to further weigh models based on their geological feasibility.

We use a Bayesian formulation of the inverse problem. In this formulation, the state of information about the subsurface after incorporation of both a priori information and data information is completely described by the a posteriori probability density $\sigma(\mathbf{m})$ over the model space [*Tarantola and Valette*, 1982]. From $\sigma(\mathbf{m})$ it is possible to calculate the probability that the true model belongs to a given class $\mathcal{A}$ of models:

$$P(\mathbf{m} \text{ belongs to } \mathcal{A}) = \int_{\mathcal{A}} \sigma(\mathbf{m}) d\mathbf{m},$$

The a posteriori probability density is the complete solution to the inverse problem [*Tarantola and Valette*, 1982]. It contains all the available prior information such as the approximate sizes of reflection coefficients and layer thicknesses, and all the data information, as "seen through the glasses" of the theoretical relationship between model and data in the form of the wave equation. In the Bayesian analysis, all the input information is preserved and no uncontrolled subjective bias is introduced.

The a posteriori probability distribution for the inverse problem is given by

$$\sigma(\mathbf{m}) = \frac{\rho(\mathbf{m})\ L(\mathbf{m})}{\int_M dm^1 dm^2 \ldots\ \rho(\mathbf{m})\ L(\mathbf{m})} . \qquad (1)$$

[*Tarantola and Valette*, 1982]. The a posteriori probability density $\sigma(\mathbf{m})$ equals (except for a normalization constant) the a priori probability density $\rho(\mathbf{m})$ times a likelihood function $L(\mathbf{m})$ measuring the fit between observed data and synthetic data calculated from the model $\mathbf{m}$.

The likelihood function is typically of the form

$$L(\mathbf{m}) = C \exp\left[-S(\mathbf{m})\right]$$

where C is a constant and $S(\mathbf{m})$ is a misfit function. $S(\mathbf{m})$ measures the difference between the observed

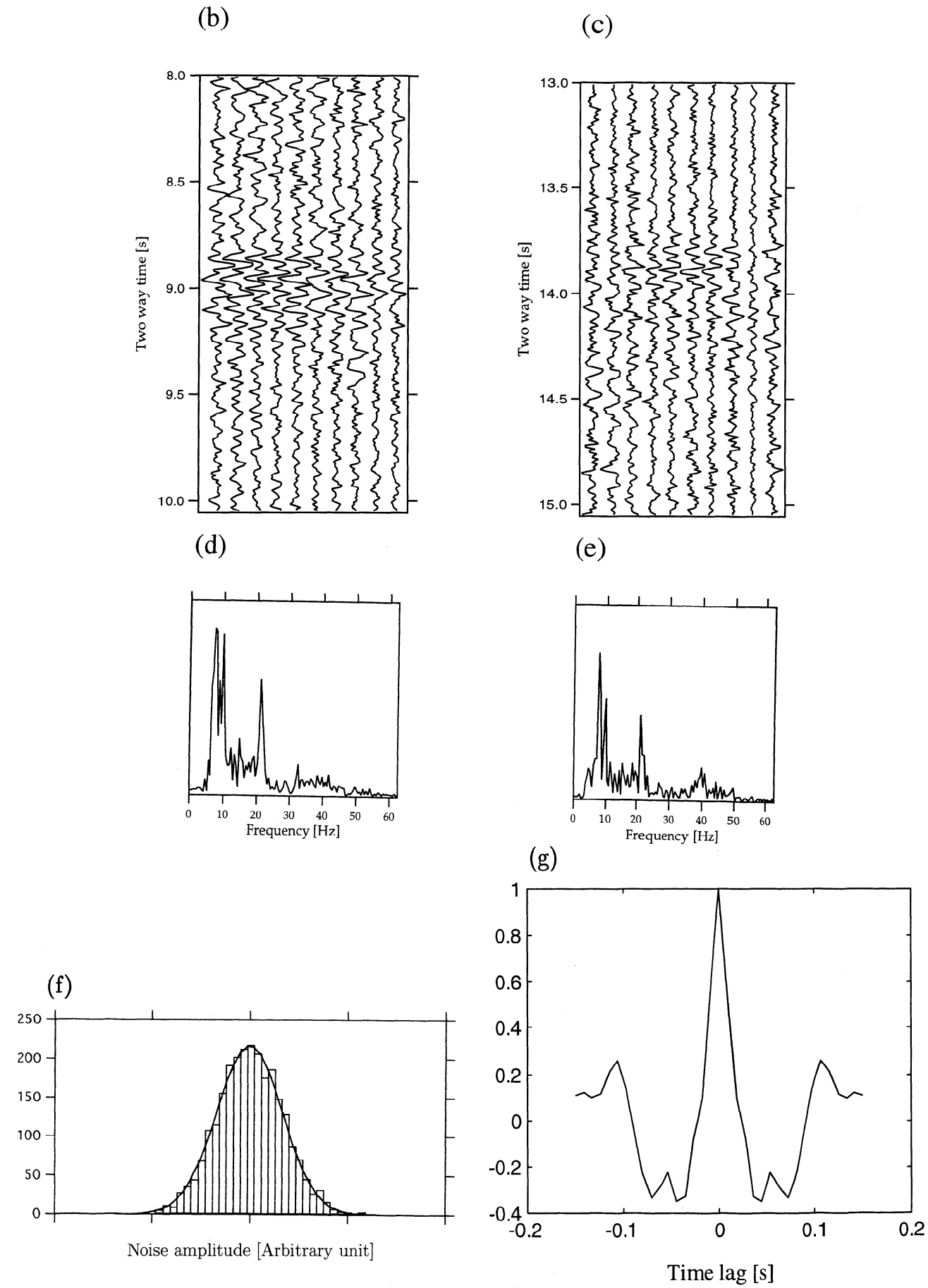

Figure 2. (continued)

data and synthetic data calculated from the model $\mathbf{m}$. If, for instance, the observational noise consists of independent Gaussian errors, $S(\mathbf{m})$ is proportional to the sum of squared differences between observed and calculated data values (the L_2 misfit), and the likelihood function is Gaussian. If, instead, the noise consists of independent Laplace distributed errors, $S(\mathbf{m})$ is the L_1 misfit (where squares are replaced by absolute values), and the likelihood is Laplacian.

Monte Carlo Sampling of the A Posteriori Distribution

Real, quantitative geological a priori knowledge cannot be described by means of simple mathematical expressions for $\rho(\mathbf{m})$. Such knowledge is often available as statistical information: histograms giving the occurrence frequency of, for instance, certain lithologies or physical rock parameters, observed in outcrops or nearby wells.

Mosegaard and Tarantola [1995] provide a method for Bayesian Monte Carlo inversion that overcomes this problem. This method has two major advantages, as compared to previously published methods [e.g., *Stoffa and Sen,* 1991]. First of all, the method is exact in the sense that it will provably sample the posterior probability density. Second, it allows incorporation of arbitrarily complex statistical a priori information into the inversion.

The algorithm consists essentially of two interacting parts. The first part is an a priori model generator that is able to produce random subsurface models, consistent with the available a priori knowledge. Consistency here means that the generated models have exactly the same statistical properties as those we have obtained from observations in the real Earth. The models produced by the a priori model generator are fed into the second part, an algorithm that decides if the a priori model can pass a data fitting test.

One iteration of the algorithm runs as follows: First, given the current model, a new model is chosen by the a priori model generator (by perturbing the current model), and the probability for a given new model to be chosen is proportional to its a priori probability. The new model $\mathbf{m}_{\text{new}}$ is now accepted or rejected according to the following rule:

1. If the value of the likelihood $L(\mathbf{m}_{\text{new}})$ of the new model is larger than or equal to the likelihood $L(\mathbf{m}_{\text{cur}})$ of the current model, the model $\mathbf{m}_{\text{new}}$ is accepted with probability 1.

2. If the value of the likelihood $L(\mathbf{m}_{\text{new}})$ is smaller than the likelihood $L(\mathbf{m}_{\text{cur}})$, the model $\mathbf{m}_{\text{new}}$ is accepted (as the next "current model") only with probability

$$P_{\text{accept}} = \frac{L(\mathbf{m}_{\text{new}})}{L(\mathbf{m}_{\text{cur}})}.$$

If the new model is rejected, the current model also becomes the next current model.

The series of "current models" produced by this two-part algorithm are, asymptotically, samples from the a posteriori distribution $\sigma(\mathbf{m})$ [*Mosegaard and Tarantola,* 1995]. After a large number of iterations, the number of times a given model $\mathbf{m}$ occurs in the collection of "current models" is approximately proportional to $\sigma(\mathbf{m})$. A large collection of such samples from $\sigma(\mathbf{m})$ provides the raw material from which various characteristics of the models can be obtained [*Mosegaard and Tarantola,* 1995]. A set of statistically independent samples of the accepted models allows structures in the subsurface that are well-resolved to be distinguished from those that are ill-resolved. A well-resolved structure will appear in most of the accepted models, whereas an ill-resolved structure will appear in only a few models. The probability that a certain structure exists is roughly proportional to its frequency of occurrence in the set of a posteriori samples. Therefore approximate a posteriori probability distributions for model parameters can be represented by normalized histograms of the parameters values. The peak of the histogram will be at the most probable model parameter, and the deviation from this peak will provide a measure of uncertainty.

Monte Carlo Sampling of Lithosphere Reflectivity

We use the Bayesian Monte Carlo algorithm described above to generate reflectivity models for selected parts of the DRUM reflection profile. We have concentrated our efforts only at a location (Figure 1) where the Moho and W reflectors are brightest and subhorizontal as the algorithm requires large computation time. We have analyzed a total of 60 unprocessed traces in the interval 8.0 s - 10.0 s TWT bracketing the Moho and the interval 13.0 - 15.0 s covering the "W reflector." We chose the 60 traces from one shot gather (3564) with the best signal to noise ratio among 10 neighboring shot records. The receiver group spacing was 50 m along a 3000-m-long streamer. The raw shot gather shows coherent energy between 13.7 s and 14.2 s TWT for the W reflector (Figure 2a). To increase the signal to noise ratio, we applied a correction for dip move out and stacked six adjacent traces, yielding 10 traces for the inversion (Figures 2b and 2c). The normalized frequency spectra show dominant energy between 6 and 30 Hz (Figure 2d and 2e). Since the Moho and W reflectors are subhorizontal and are at large depths, the incident seismic waves are essentially vertically traveling plane waves. It is therefore possible to perform a rather careful calculation of synthetic seismograms using a fast one-dimensional propagator matrix method [*Haskell,* 1953].

Wavelet Estimation

The DRUM profile was shot by GECO (Geophysical Company of Norway) using an 8536-cubic-inch air gun array at 7.5 m below the sea surface [*McGeary and Warner,* 1985]. A simulated far-field source signature

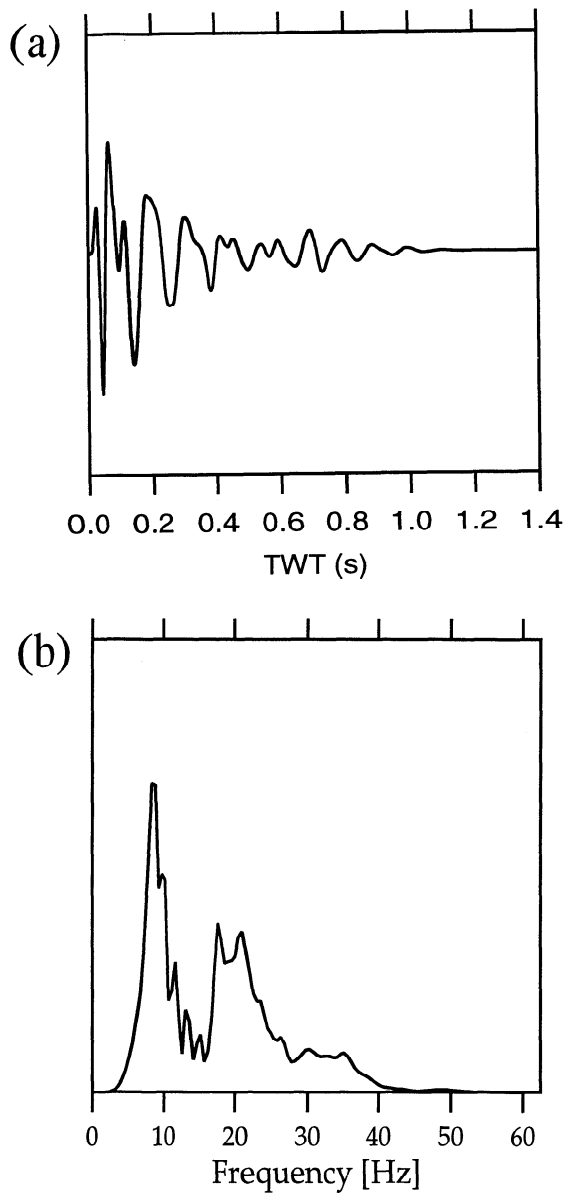

Figure 3. (a) The source wavelet used in the inversion. This trace represents a simulated far-field source signature for the entire air gun array provided by the contractor (GECO), convolved with the receiver ghost, recording filter, and reverberations within the 55-m-thick water layer. The wavelet was then propagated to the appropriate two-way travel time using a quality factor of 500 to approximate effects of attenuation. (b) The associated frequency spectrum.

for the air gun configuration used in the experiment, provided by GECO, was used in this study. Since the streamer was at 17-m depth, the source wavelet was convolved with the appropriate receiver ghost and was then filtered using a minimum phase band-pass filter, 5.3 Hz at 18 dB/octave to 45 Hz at 72 dB/octave, the filter used in recording the data. The effect of reverberations in the water layer at both the source and receiver ends of the ray path was included in the source wavelet. This estimate used a water depth of 55 m measured by an echo sounder during the survey, and a water-seabed reflection coefficient of 0.5 and a water velocity of 1.5 km/s determined using refracted arrivals from the seabed that were observed in shot gathers. The resulting source wavelet was propagated down to 8 s for the Moho and to 13 s for the W reflector, and the effect of attenuation was incorporated using a quality factor of 500 [*Hobbs and Snyder,* 1993] (Figure 3).

The size of the inverse problem was in this way reduced by focusing only on two zones, each of 2 s (TWT), containing the Moho or W reflections. In the calculation of synthetic seismograms it was assumed that the response from each interval considered depended on the overlaying layers (the overburden) only via the propagation effects built into the source wavelet. We neglected in this approximation all multiples in the earth that involve reflectors in the overburden. These multiples are considered negligible due to the rather small reflection coefficients (no more than 0.1) generally assumed to be present in the lithosphere [*Holbrook et al.,* 1992] and the presence of attenuation in the Earth.

A Priori Information

Reflections from deep in the lithosphere require large impedance contrasts. The simplest approach is to treat each reflection as originating at the boundary of a layer overlying a half space and then estimate reflectivity, which could be due to either a positive or negative impedance contrast. Such an approach is appropriate when a reflection is sharp and distinct and the data have no noise. In practice, reflections consist of a series of events, which cannot be distinguished, and often contain considerable noise. In such cases, this simple model is inappropriate and additional information is required.

To obtain appropriate a priori information on the structure of deep reflections, we considered the possible geological processes which might be responsible for these reflectors. These are widely considered to include layered mafic intrusions, shear zones with possible metasomatic residuals enhancing reflectivities, or alternating types of metamorphic rocks [*Mooney and Meissner,* 1992; *Clowes and Green,* 1994]. We have chosen one of these possibilities as a basis for generation of a priori models: layered igneous intrusions in a large magma chamber formed by fractional crystalization of magma derived from the mantle [*Weibe,* 1993]. Physical properties of rocks found in the igneous intrusive complexes of Rum, an island west of Scotland, and Great Dyke in Zimbabwe form the basis of our quantitative a priori information [*Singh and McKenzie,* 1993]. We have only used that part of the information from the igneous complexes that is expected to be fairly independent of the depth of burial, that is, reflection coefficients and layer thicknesses. In other words, there are no constraints on the absolute acoustic impedance values in our calculations. Any other plausible geolog-

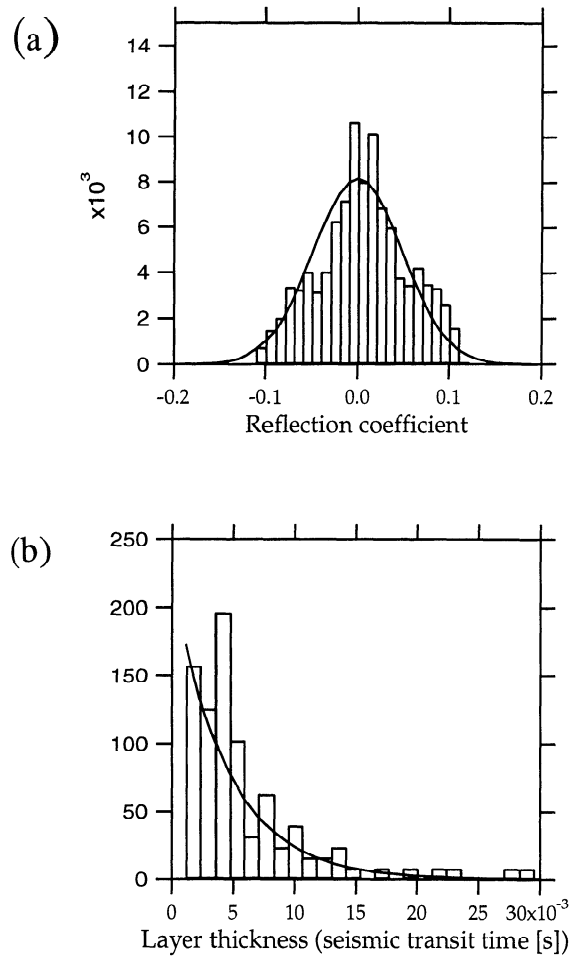

Figure 4. A priori information used by the a priori model generator in the first stage of the Bayesian inversion scheme. (a) Reflection coefficients distribution obtained from studies of the igneous intrusions of Rum, Scotland, and the Great Dyke, Zimbabwe [*Singh and McKenzie,* 1993], that are consistent with other studies such as those of the Pleasant Bay layered gabbro-diorite [*Weibe,* 1993]. The solid curve has a Gaussian distribution with standard deviation $\sigma = 0.047$. (b) Layer thickness distribution as a function of one-way travel time derived from observations of the Rum and Great Dyke intrusions. The solid curve has an exponential distribution with $\lambda = 225.0\ s^{-1}$.

ical model could have been used as prior information, but the igneous intrusions have been more thoroughly mapped on the surface and relevant statistics are available with greater detail than for either shear zones or metamorphic layering.

Histograms (Figure 4) illustrate the distributions of reflection coefficients and the layer thicknesses for these intrusive complexes that guided our a priori model generator. The thicknesses of the layers have been converted from meters into seconds using the velocity in each layer derived from the modal composition [*Singh and McKenzie,* 1993]. In order to retain only the general features of the reflectivity and thickness histograms, they were approximated with a Gaussian and an exponential distribution, respectively. In this way we avoided detailed histogram structure that is only characteristic of the specific igneous intrusion complexes considered in this study. All a priori models generated by our algorithm are consistent with the approximate distributions; that is, histograms of reflection coefficients and layer thicknesses produced from these models are statistically equivalent to corresponding histograms from the igneous complexes. The combined a priori distribution used here allows models with reflection coefficients ranging from about -0.1 to +0.1 and thicknesses from about 10 m to 2000 m.

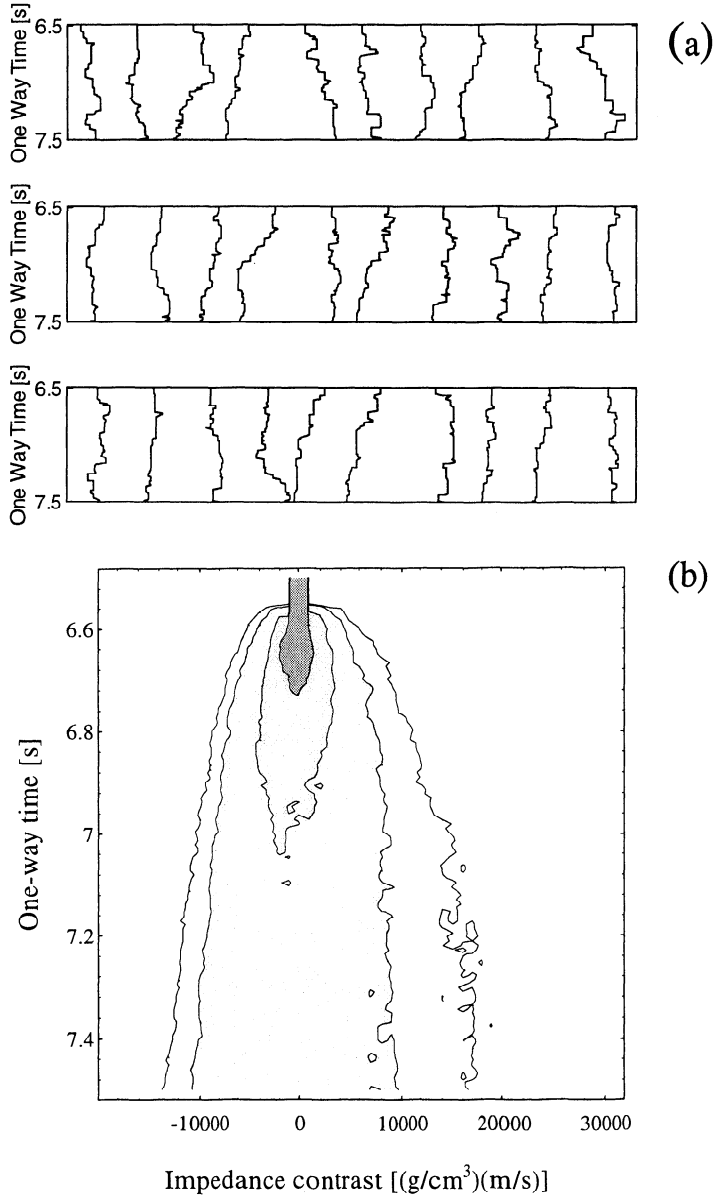

Figure 5. (a) A selection of typical a priori models generated assuming the distributions shown in Figure 4. These models are all statistically equivalent and have equal likelihoods of existence. (b) Marginal a priori impedance contrast distributions for all one-way times in a 1-s interval.

Figure 5 shows a selection of a priori impedance models generated using the statistics derived from Figure 4 for the igneous intrusions. All the a priori models are different, but they all have identical statistics. These impedance models have been calculated from their corresponding reflectivity models, and for comparison, all models have the same impedance value, 19,000 m/s(g/cm^3), at the top. Under this assumption, the weakness of the constraints on the absolute acoustic impedance values can be observed directly, since unrealistically high and low values of impedance occur (Figure 5). Consequently, our a priori information will provide no strong impedance constraints on the results of our calculations.

Model Parameterization and Calculation of Synthetic Seismograms

The complexity of the a priori information means that $\rho(\mathbf{m})$ and hence $\sigma(\mathbf{m})$ deviate strongly from a Gaussian distribution. Consequently, the inverse problem is not easily analyzed by conventional, linearized methods. In particular, a correct, nonlinear error and resolution (nonuniqueness) analysis may only be possible through a Monte Carlo approach.

We employed a Monte Carlo technique for inversion, and therefore a fast computation of synthetic seismograms was required in order to be efficient. Synthetic seismograms were computed using a propagator matrix method [*Ganley*, 1981]. All multiple reflections, absorption, and dispersion within the target zones were incorporated. Dispersion was derived from Q, using a dispersion model given by *Futterman* [1962].

To further speed up the Monte Carlo inversion, model parameterization consisted of reflection coefficients specified as a function of one-way travel time. As the relation between reflectivity and data is only moderately nonlinear, this parameterization (and the fact that the noise is Gaussian) makes $L(\mathbf{m})$ become close to a Gaussian. Consequently, the inverse problem is easier to solve. Each model consists of 128 reflection coefficients with a sampling interval of 0.008 s.

Data Noise and the Likelihood Function $L(\mathbf{m})$

Each of the data sets considered consists of 10 neighboring traces of 2.048-s length (Figure 2b and 2c). Because coherent events in the data sets are approximately horizontal and laterally invariant, we estimated the incoherent noise in the data by first finding one of the best fitting horizontally stratified models for the data set. The (10 identical) vertical incidence traces computed from this model were then subtracted from the 10 data traces to form corresponding error traces, the 10 noise traces. These noise traces were all fairly similar, stationary signals, and the distribution of noise values was very close to a Gaussian. Since the data noise has a Gaussian distribution, we define the likelihood function as

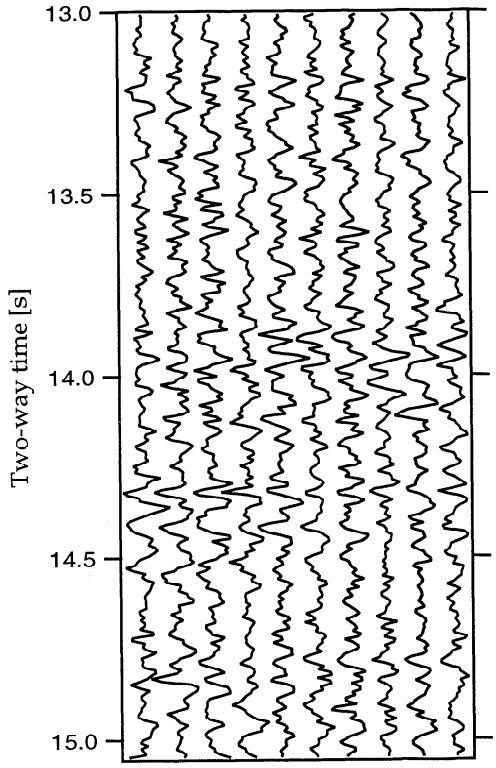

Figure 6. Noise contaminated, synthetic data used to test the algorithm. The noise (and signal to noise ratio) is equal to the noise extracted from the Moho data.

$$L(\mathbf{m}) = \exp\left\{-\frac{1}{2}\left[\mathbf{g}(\mathbf{m}) - \mathbf{d}_{\text{obs}}\right]^T \mathbf{C}_d^{-1}\left[\mathbf{g}(\mathbf{m}) - \mathbf{d}_{\text{obs}}\right]\right\}, \tag{2}$$

where $\mathbf{C}_d$ is the covariance matrix for the noise. For the Moho data and W reflector data we found signal to noise (amplitude) ratios of 1.9 and 1.4, respectively. The estimated marginal distribution of a single noise value is shown in Figure 2f, and the estimated noise autocorrelation (normalized to one at zero lag) is shown in Figure 2g.

Synthetic Example

Our algorithm was calibrated and tested on synthetic data from a known subsurface model. The synthetic test was designed to mimic a situation similar to the analysis of the Moho reflector. The DRUM source wavelet was used, and the noise extracted from the Moho reflector data was added to the synthetic traces to form an artificial, noisy data set (Figure 6).

We ran 100,000 iterations of the Monte Carlo inversion on the synthetic data set. The models were generated according to the a priori information derived from the igneous complexes of Rum and Great Dyke (Figure 4). The second part of the Monte Carlo algorithm, accepting or rejecting models proposed by the a priori model generator, used a likelihood function defined by (2) with a noise variance corresponding to a signal to noise ratio of 1.9, the signal to noise ratio of the Moho reflector data.

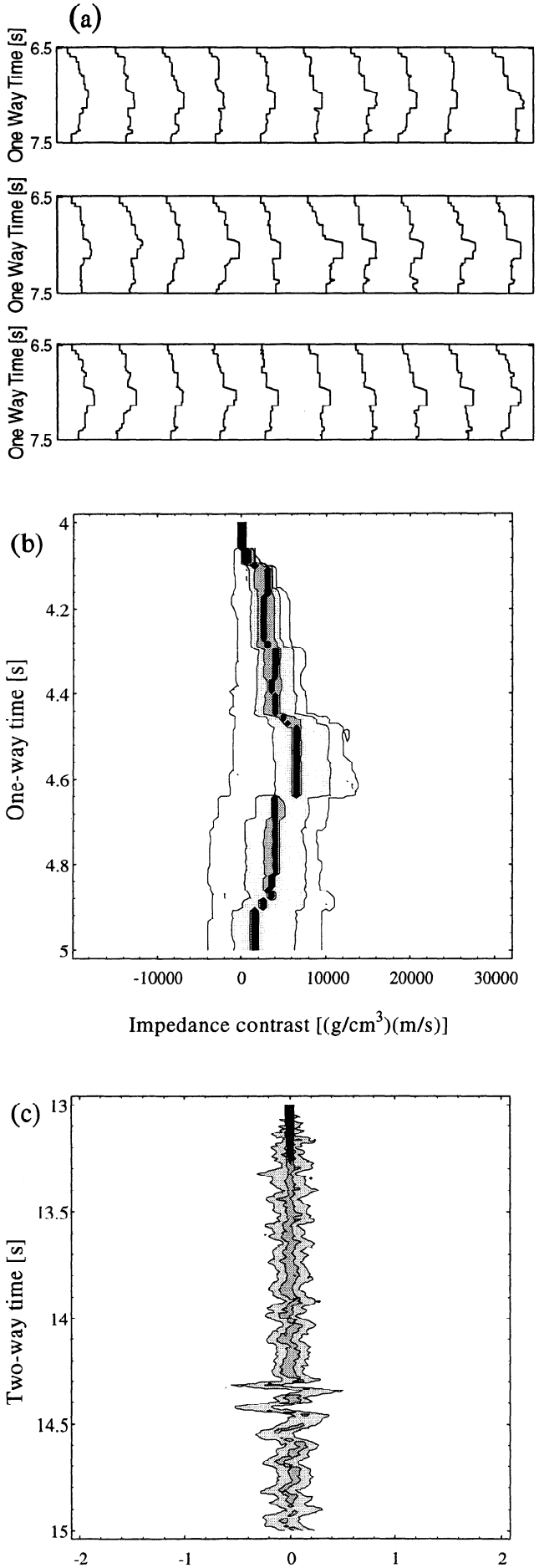

In each iteration, all 128 reflection coefficients are considered by the algorithm. Each of the reflection coefficients are perturbed by the a prior model generator, and the perturbed model is accepted or rejected according to the rule given above. The series of "current models" produced by this algorithm are samples from the a posteriori distribution $\sigma(\mathbf{m})$. The strategy of perturbing only one reflection coefficient at a time preserves most characteristics of the current model, which may have fitted the data well. This strategy is efficient, since we want to visit many models with a good data fit, but it provides models that are successively correlated. This is a problem since error and resolution analysis requires a collection of statistically independent models from the a posteriori distribution. A smaller set of models chosen from among the accepted models in such a way that they are sufficiently separated in time (iterations) constitutes such a set of independent models. Here, as in the analyses of the field data below, we chose to save only every hundredth model. This waiting time of 100 iterations between accepted models was found by analyzing the fluctuations of $L(\mathbf{m})$ as the iterations proceeded. Inspection of the autocorrelation function for these fluctuations showed that accepted models separated by a hundred iterations were unlikely to be correlated. Thus we have 1000 independent samples of the a posteriori distribution from 100,000 sampled models.

The results are shown in two ways. Figure 7a shows the original model used to generate the synthetic data in the upper left corner together with a selection of a posteriori models, randomly selected from the 1000 a posteriori models selected by the algorithm. Since these models are randomly chosen from the 1000 independent samples of the posteriori models, they roughly approximate the a posteriori distribution. In Figure 7c, the distribution of synthetic data is shown. All the synthetic traces are statistically indistinguishable from the reference trace calculated from the original impedance model, in that their deviations from this noise trace are within the noise level.

The variations in the model that are obtained by the Monte Carlo inverion, and hence permitted by the a priori information and the data, are evident. To interpret this output correctly, it should be remembered that the method is designed to produce particular model features with a frequency proportional to their a poste-

Figure 7. The results of the inversion on the synthetic data. (a) The true model (the curve at the upper leftmost corner) and a selection of a posteriori models. (b) Marginal a posteriori impedance contrast distributions for all one-way times between 6.5 and 7.5 s. (c) Marginal a posteriori data distributions for all two-way times between 13.0 and 15.0 s. Since all impedance models are fixed at 19,000 g/cm^3(m/s) near 13.0 s, these distributions approach a delta function at the top of the figure.

riori probability. This means that the probability of a feature that exists in the impedance model is roughly proportional to the number of times the feature occurs on Figure 7a. If it appears on almost all the a posteriori models, it is well resolved. It is clear from Figure 7a that, for instance, the high impedance zone between 6.950 and 7.150 s is well resolved. The actual impedance contrast value between the interior of the zone and its surroundings (above and below) shows some variation between the a posteriori models and is therefore poorly resolved.

Of particular interest to this study is the overall impedance contrast, that is, the increase in impedance from the top to the bottom of the zone. In Figure 7b, the marginal a posteriori distributions for impedance contrasts at all the considered depths are shown. It is clear from this figure that the magnitude of the overall change in impedance is poorly resolved. However, the polarity (sign) of the overall impedance contrast is well resolved. As seen from the impedance contrast distribution at 7.5 s one-way time, it has a very high probability of being positive, in agreement with the original model (shown in black in the figure).

Moho

A similar analysis of the actual Moho data from the DRUM profile results in the a posteriori models shown in Figure 8a and 8b, respectively. Due to the fact that the estimated wavelet may be in error by an unknown, constant scaling factor k, the only information we can extract from the data is the ratio between impedance contrast $\Delta I(T)$ and k. The impedance contrast is the impedance at one-way time T minus impedance at the top of the target zone. See the Appendix for further details on this problem. Figure 8a shows this ratio as a function of one-way travel time in the target zone. Figure 8b shows estimated marginal a posteriori distributions for impedance contrasts at all depths in the considered interval.

An inspection of the a posteriori Moho models (Figure 8a) shows a well-resolved layered sequence having a thickness of about 0.3 ± 0.04 s one-way time, equivalent to approximately 2.4 ± 0.6 km. Impedances alternately increase and decrease within the series, but overall the series has a cumulative increase. The observed, well-resolved, positive polarity of the overall impedance contrast for this interval (Figure 8b) is consistent with previous refraction results that used diving rays and wide-angle reflections to model observed phases [*Barton*, 1992].

W Reflector

The calculated a posteriori models for the W reflector zone are shown in Figure 9a. Some well-resolved, consistent features are observed in the interval between 6.8 s and 7.3 s one-way time. Over this short interval, with an approximate thickness of 3.7 ± 0.6 km, the

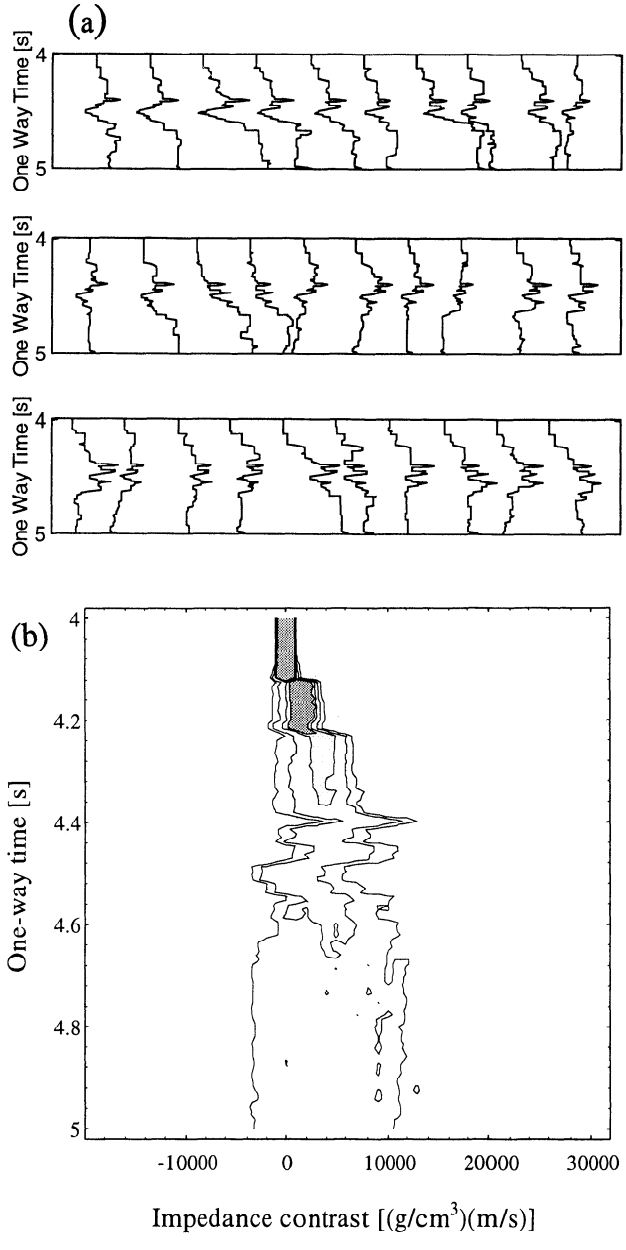

Figure 8. The results of the inversion on the Moho data set. (a) A selection of a posteriori models. (b) Marginal a posteriori impedance contrast distributions for all one-way times between 4.0 and 5.0 s.

overall change in acoustic impedance is poorly resolved (Figure 9b). The consistency of the models between 6.8 and 6.9 s indicates a high probability of negative impedance contrasts over this zone about 1.25 km thick. The greater variability of a posteriori models below 6.9 s indicates some probability for both positive and negative contrasts deeper in the interval. The polarity of the overall impedance contrast is not as well resolved as over the Moho interval described above. The marginal impedance contrast histogram at 7.5 s one-way time (Figure 9b) reveals that the a posteriori probability of a nonpositive polarity, approximated by the portion of this histogram around and to the left of the origin, is

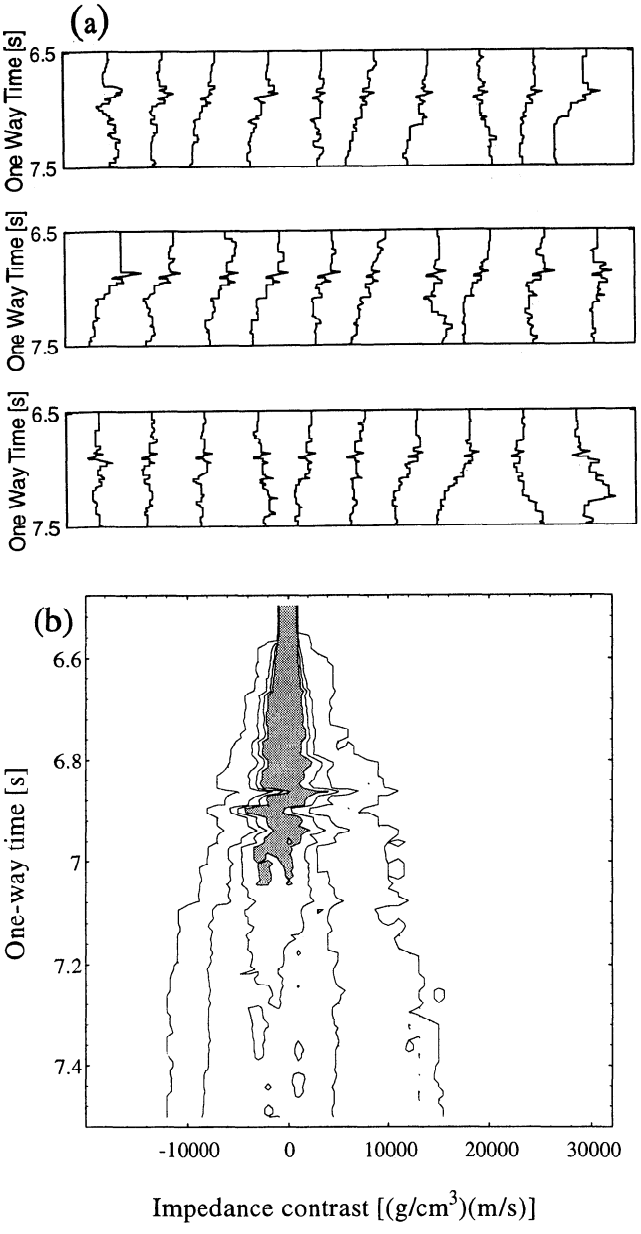

Figure 9. The results of the inversion on the W reflector data set. (a) A selection of a posteriori models. (b) Marginal a posteriori impedance contrast distributions for all one-way times between 6.5 and 7.5 s.

significantly larger than the corresponding probability of a positive polarity.

This model with an upper layer of negative impedance contrasts overlying a layer of more ambiguous but generally nonpositive impedance contrasts cannot be simply reconciled with previous estimates of velocities at a similar depth that were obtained from previous seismic surveys in the vicinity of this area [*Barton*, 1992; *Faber and Bamford*, 1979]. The LISP-B (Lithospheric Seismic Profile in Britain) seismic records showed high-amplitude P wave phases that arrived closely after first arrivals from rays diving into the uppermost mantle. These observed high-amplitude phases can be generated from post critical reflections off a layer with an increase in P wave impedance [*Barton*, 1992]. Alternatively, a zone of increased velocity several kilometers thick with no strong velocity gradients above but a steep negative gradient below can simultaneously explain the observed large amplitude P waves as well as low apparent velocity of these high-amplitude phases and the absence of any head waves [*Faber and Bamford*, 1979]. In either interpretation, the overall change in velocity over the depth range containing the W reflector will be a positive one. As previously noted, our analysis cannot resolve the overall change, but the high probability of a nonpositive contrast toward the top of the zone is closer to the original interpretation of the LISP-B data by *Faber and Bamford* [1979].

Discussion

Small-scale impedance contrasts modeled by our Monte Carlo analysis need not necessarily be consistent with broader velocity gradients sensed by previous refraction surveys. The two do seem to coincide at the Moho at $\sim$ 30-km depth, but not around the W reflector at $\sim$ 50-km depth. The model first proposed in the original interpretation of the LISP-B data [*Faber and Bamford*, 1979] might be appropriate: a gentle positive gradient underlain by a local, steep negative gradient in impedance above another gentle positive gradient. This in effect produces a layer of low impedance, about 1 km thick within a thick layer with overall high-impedance region which cannot be fully resolved by our method at present.

Other recent studies of velocity and impedance structure of the lithospheric layer associated regionally with the Flannan and W reflectors, although also non-definitive, do suggest that a positive gradient occurs at these depths [*Barton*, 1992; *Morgan et al.*, 1994]. Local negative steps in impedance or velocity cannot be excluded by any study and may help explain some features of the record sections. In some locations the analysis may have been made on a different mantle feature from that analyzed in this study. Distinctions have been made between the largely subhorizontal W reflector interpreted to have a Caledonian (400 Ma) or older origin [*Snyder and Flack*, 1990] and the dipping Flannan reflector associated with Permo-Triassic extension and basin formation [*Reston*, 1990].

A limited number of common mineral assemblages are available to produce the appropriate impedance contrasts at 50 km depths that are required by the observation (see *Snyder and Flack*, [1990]) for one recent compilation and references). Eclogite facies metamorphic rocks of gabbroic composition and peridotite are the most probable high-velocity, high-density rocks. Metasomatic deposits provide the most likely source of low-impedance material at these depths. Such deposits typically contain phlogopite mica and other exotic high-pressure minerals deposited by volatile-rich melts, as exemplified by the numerous mineral assemblages ob-

served in Kimberlite pipes in South Africa [*Schulze*, 1989]. Normal faults associated with extension and basin formation typically enhance impedance contrasts by juxtaposing high-impedance rocks below rocks of lower impedance. This provides one possible explanation for the Flannan reflector impedance models [*Morgan et al.*, 1994].

Thermotectonic processes associated with orogenies and stable cratons are more variable but can provide environments suitable for the introduction of negative impedance contrasts with increasing depth by trapping migrating melts or fluids [*Snyder and Flack*, 1990]. Here we give just two examples. In one possible model, the Moho velocity increase results from a phase transition from granulite to eclogite facies that has been steepened by subsequent horizontal shearing localized by this phase transition. The W reflector might then result from a diffuse transition from eclogitic rocks to peridotite, a compositional boundary. Another possible model produces the Moho reflections from a compositional change from a gabbroic granulite to peridotite. Very local negative impedance contrasts associated with the W reflector would then require an anomalous layer imbeded within the peridotite: perhaps a thin, phlogopite-rich metasomatic layer in contact with a mafic intrusive now in eclogite metamorphic facies. The most probable impedance distributions from our Monte Carlo analysis can be interpreted by making reasonable geological assumptions about metasomatic processes and metamorphic grade. That does not necessarily make them correct.

Conclusions

We have provided a strategy for determining polarity of complex reflectors from normal-incidence data. The strategy is based on the Bayesian inversion theory. It consists of two steps: (1) a priori model generator where any type and any number of a priori probability distributions can be used and (2) selection of the model based on fit between synthetic and observe data. We applied this analysis to intriguing features in the mantle beneath northern Scotland that will undoubtedly never be directly sampled to confirm our models and interpretations. Given the uncertainties of the inversion method and the small amount of suitable data that is available with sufficient signal-to-noise ratios to be useful, we feel that the results must first be assessed independently and demonstrated to be reliable and self-consistent. Similar analysis of wide-angle (postcritical) reflections could provide additional new constraints for example but would then only strengthen our present conclusions if the results compared favorably.

As the depth increases, the Moho contains largely positive impedance contrasts, and the W reflector is likely to display a negative or zero overall impedance contrast, at least in its upper levels. This latter conclusion is new and significant information about mantle reflectors. Candidate materials exist which produce both positive and negative impedance contrasts, but to confidently distinguish between the two is an important first step.

Appendix: The Influence of Wavelet Scaling Error on Computed Impedance Functions

For small reflection coefficients (which we have in our case, where $r_i \leq 0.1$), the acoustic impedance $I(T)$ is related to the reflectivity $r(T)$ through [*Peterson et al.*, 1955]

$$I(T) \approx I_0 \exp\left[\frac{2}{\Delta T}\int_0^T r(u)du\right] .$$

where ΔT is the sampling interval for $I(T)$ and $r(T)$ and I_0 is the impedance at the top ($T = 0$) of the considered interval. Let us now look at the acoustic impedance function $\hat{I}(T)$ we obtain if the wavelet is in error with a scale factor k. In that case the computed reflectivity $\hat{r}(T)$ is related to the real reflectivity $r(T)$ through $\hat{r}(T) = r(T)/k$. We get

$$\hat{I}(T) \approx I_0 \exp\left[\frac{2}{\Delta T}\int_0^T \frac{1}{k} r(u)du\right] .$$

The relationship between $\hat{I}(T)$ and $I(T)$ is now

$$\frac{\hat{I}(T)}{I_0} \approx \exp\left[\frac{2}{\Delta T}\int_0^T \frac{1}{k} r(u)du\right] \approx \left[\frac{I(T)}{I_0}\right]^{\frac{1}{k}} .$$

Since

$$x^{\frac{1}{k}} \approx 1 + \frac{1}{k}(x-1)$$

for x close to 1, we get the following simple, approximate relation between scaled and unscaled impedance:

$$\frac{\hat{I}(T)}{I_0} \approx 1 + \frac{1}{k}\left[\frac{\hat{I}(T)}{I_0} - 1\right]$$

or

$$k\Delta\hat{I} \approx \Delta I$$

where $\Delta I = I(T) - I_0$ is the impedance contrast over the considered interval.

Acknowledgments. The authors are indebted to Associate Editor John Scales for his valuable suggestions and criticism. K. Mosegaard has received financial support from BIRPS and from Danish Natural Science Research Council (SNF). H. Wagner has received financial support from SNF. BIRPS is funded by the Natural Environment Research Council and BIRPS Industrial Associates (Amerada-Hess Ldt., BP Exploration Co. Ldt., Chevron UK Ltd., Conoco (UK) Ltd., Lasmo North Sea Plc., Mobil North Sea Ltd., Shell UK Exploration and Production). This is University of Cambridge Department of Earth Sciences contribution 4757.

References

BABEL Working Group, Integrated seismic studies of the Baltic Shield using data in the Gulf of Bothnia region, *Geophys. J. Int.*, *112*, 305–324, 1993.

Barton, P., LISP-B revisited, A new look under the Caledonides of northern Britain, *Geophys. J. Int.*, *110*, 371–391, 1992.

Clowes, R. M., and A. G. Green (Eds.), Seismic reflection probing of the continents and their margins, *Tectonophysics*, *232*, 450 pp., 1994.

Clowes, R. M., F. A. Cook, A. G. Green, C. E. Keen, J. N. Ludden, J. A. Percival, G. M. Quinlan, and G. F. West, LITHOPROBE New perspectives of crustal evolution in Canada, *Can. J. Earth Sci.*, *29*, 1813–1864, 1992.

Faber, S., and D. Bamford, Lithospheric structural contrasts across the Caledonides of northern Britain, *Tectonophysics*, *56*, 17–30, 1979.

Futterman, W.I., Dispersive body waves, *J. Geophys. Res.*, *67*, 5279–5291, 1962.

Ganley, D.C., A method for calculating synthetic seismograms which include the effects of absorption and dispersion, *Geophysics*, *46*, 1100–1107, 1981.

Haskell, N. A., The dispersion of surface waves from point sources in a multilayered media, *Bull. Seismol. Soc. Am.*, *43*, 17–34, 1953.

Hobbs, R., and D. Snyder, Marine seismic sources used for deep seismic reflection profiling, *First Break*, *10*, 417–428, 1993.

Holbrook, W.S., W.D. Mooney, and N. I. Christensen, The seismic velocity structure of the deep continental crust, in *Continental Lower Crust, Dev. Geotectonics*, vol. 23, edited by D.M. Fountain, R. Arculus, and R.W. Kay, pp. 1-34, Elsevier, New York, 1992.

Jannane, M., et al., Wavelengths of structures that can be resolved from seismic reflection data, *Geophysics*, *54*, 906–910, 1989.

Klemperer, S. L., and R. Hobbs, *The BIRPS Atlas: Deep Seismic Reflection Profiles across the British Isles*, 124 pp., Cambridge Univ. Press, New York, 1991.

McGeary, S., and M. R. Warner, Seismic profiling of the continental lithosphere, *Nature*, *317*, 795–797, 1985.

Mooney, W.D., and R. Meissner, Multi-genetic origin of crustal reflectivity: a review of seismic reflection profiling of the continental lower crust and Moho, in *Continental Lower Crust, Dev. Geotectonics*, vol. 23, edited by D.M. Fountain, R. Arculus, and R.W. Kay, pp. 45-79, Elsevier, New York, 1992.

Morgan, J. V., M. Hadwin, M. R. Warner, P. J. Barton, and R. P. L. Morgan, The polarity of deep seismic reflections from the lithospheric mantle: Evidence for a relic subduction zone, *Tectonophysics*, *232*, 319–328, 1994.

Mosegaard, K., and A. Tarantola, Monte Carlo sampling of solutions to inverse problems, *J. Geophys. Res.*, *100*, 12,431-12,447, 1995.

Peterson, R.A., W.R. Fillipone, and F.B. Coker, The synthesis of seismograms from well log data, *Geophysics*, *20*, 516–538, 1955.

Reston, T. J., The lower crust and extension of the continental lithosphere: Kinematic analysis of BIRPS deep seismic data, *Tectonics*, *9*, 1235–1248, 1990.

Schulze, D. J., Constraints on the abundance of eclogite in the upper mantle, *J. Geophys. Res.*, *94*, 4205–4212, 1989.

Singh, S. C., and D. P. McKenzie, Layering in the lower crust, *Geophys. J. Int.*, *113*, 622–628, 1993.

Snyder, D., and C. A. Flack, A Caledonian age for reflectors within the mantle lithosphere north and west of Scotland, *Tectonics*, *9*, 903–922, 1990.

Stoffa, P. L., and M. K. Sen, Nonlinear multiparameter optimization using genetic algorithms: Inversion of plane-wave seismograms, *Geophysics*, *56*, 1794–1810, 1991.

Tarantola, A., and B. Valette, Inverse problems = quest for information, *J. Geophys.*, *50*, 159–170, 1982.

Weibe, R. A., The Pleasant Bay layered gabbro-diorite, coastal Maine: Ponding and crystallization of basaltic injections into a silicic magma chamber, *J. Petrol.*, *34*, 461–489, 1993.

Zhao, W., K. D. Nelson, and Project INDEPTH Team, Deep seismic reflection evidence for continental underthrusting beneath southern Tibet, *Nature*, *366*, 557–559, 1993.

Klaus Mosegaard and Helle Wagner, Dept. of Geophysics, Niels Bohr Institute for Astronomy, Physics and Geophysics, Juliane Maries Vej 30, DK-2200 Copenhagen , Denmark. (e-mail: klaus@gfy.ku.dk; hw@miraculix.gfy.ku.dk)

Satish Singh and David Snyder, British Institutions Reflection Profiling Syndicate, Bullard Laboratories, University of Cambridge, Cambridge, England. (e-mail: singh@esc.cam.ac.uk; snyder@esc.cam.ac.uk)

(Received July 16, 1996; accepted August 13, 1996.)